Journal of Power Sources 195 (2010) 1454–1462

Contents lists available at ScienceDirect

Journal of Power Sources

journal homepage: www.elsevier.com/locate/jpowsour

Experimental investigation of 1 kW solid oxide fuel cell system with a natural gas reformer and an exhaust gas burner

Tzu-Hsiang Yen*, Wen-Tang Hong, Wei-Ping Huang, Yu-Ching Tsai, Hung-Yu Wang, Cheng-Nan Huang, Chien-Hsiung Lee

Institute of Nuclear Energy Research Atomic Energy Council, Taoyuan County 32546, Taiwan

ARTICLE INFO

Article history:
Received 30 July 2009
Received in revised form 8 September 2009
Accepted 9 September 2009
Available online 16 September 2009

Keywords:
Solid oxide fuel cell
After-burner
Combined heat and power

ABSTRACT

An experimental investigation is performed to establish the optimal operating conditions of a porous media after-burner integrated with a 1 kW solid oxide fuel cell (SOFC) system fed by a natural gas reformer. The compositions of the anode off-gas and cathode off-gas emitted by the SOFC when operating with fuel utilizations in the range 0–0.6 are predicted using commercial GCTool software. The numerical results are then used to set the compositions of the anode off-gas and cathode off-gas in a series of experiments designed to clarify the effects of the fuel utilization, cathode off-gas temperature and excess air ratio on the temperature distribution within the after-burner. The experimental results show that the optimal after-burner operation is obtained when using an anode off-gas temperature of 650 °C, a cathode off-gas temperature of 390 °C, a flame barrier temperature of 700 °C, an excess air ratio of 2 and a fuel utilization of $U_f = 0.6$. It is shown that under these conditions, the after-burner can operate in a long-term, continuous fashion without the need for either cooling air or any additional fuel other than that provided by the anode off-gas.

1. Introduction

Due to mounting concerns regarding the potentially catastrophic effects of global warming and dwindling oil resources, an urgent requirement exists for highly efficient, environmental-friendly power generation systems. Solid oxide fuel cells (SOFCs), which produce electrical energy by oxidizing a suitable fuel, have emerged as a feasible means of satisfying this requirement for a wide variety of applications ranging from simple auxiliary power units to large-scale power generation systems. SOFCs have high electrical efficiency (40–60%), low emissions, the ability to operate on a wide variety of different fuels, and the potential for implementation in an integrated gasification combined cycle (IGCC) to accomplish SOFC coal-based central power plants [1–3]. In order to ensure an adequate ionic and electronic conductivity of their components, SOFCs are required to operate at very high temperatures (e.g. 650–1000 °C). The high operation temperature needs longer start-up time. Although it needs a longer start-up time, the high operating temperature has a number of significant advantages including the ability to reform the fuel directly without the need for a catalyst and the potential to utilize the high-temperature by-product gases for secondary purposes such as driving an auxiliary electrical generation plant (e.g. a turbine system) or feeding decentralized energy systems. Such hybrid systems, generally referred to as combined heat and power (CHP) systems, enable an overall efficiency of as much as 90% to be obtained. Santangelo and Tartarini [4] compared the fuel consumption characteristics of fuel cells and traditional power generation systems and suggested that fuel cell devices provided the potential for developing CHP systems for residential and industrial applications with virtually complete energetic independence. Chung et al. [5,6] investigated the effects of energy recuperation on the efficiency of a SOFC and showed that the overall system efficiency could be increased from 50% to 68% by recirculating the partial fuel and steam from the anode exhaust of the SOFC.

Finnerty et al. [7] presented a novel three-way catalytic fuel processing system for SOFC power plants consisting of a pre-reformer catalyst, a fuel cell anode catalyst and a platinum-based combustor. The results showed that the proposed system was capable of processing either methane or butane as the SOFC fuel. Chan et al. [8] presented two simple SOFC power systems fed by hydrogen and methane, respectively, in which the wasted heat was recovered by an after-burner and used to preheat the fuel and air prior to their ingress into the SOFC. The experimental results revealed that the addition of the after-burner to the SOFC system increased the overall efficiency of the system by around 70%.

Fontell et al. [9] designed and constructed a 1–5 kW SOFC system. The system showed that an effective reduction in the harmful emissions could be obtained for various fuel compositions by maintaining the flue gas temperature at around 700 °C by using a

* Corresponding author. Tel.: +886 3 4711400x2953; fax: +886 3 4711409.
E-mail address: occasion@mail.tn.edu.tw (T.-H. Yen).

0378-7753/$ – see front matter © 2009 Elsevier B.V. All rights reserved.
doi:10.1016/j.jpowsour.2009.09.021

Nomenclature

c_p	specific heat capacity ($J\,m^{-3}\,K^{-1}$)
d_m	equivalent porous cavity diameter (m)
e_o	standard state potential for cell (V)
F	Faraday's constant (96,485 $C\,mol^{-1}$)
G	free energy ($kJ\,mol^{-1}$)
H	enthalpy ($kJ\,mol^{-1}$)
I	cell current (A)
m	mass flow rate ($kg\,s^{-1}$)
P_{elec}	total electrical power for cells (W)
Pe	Péclet number
PH-A	pre-heater for air
PH-F	pre-heater for fuel
PH-S	pre-heater for steam
PSV	proportional solenoid valve
m_{fuel}	fuel of mass flow rate ($kg\,s^{-1}$)
m_{ox}	oxygen mass flow rate ($kg\,s^{-1}$)
n_{O_2}	oxygen molar flow rate ($mol\,s^{-1}$)
S	entropy ($kJ\,mol^{-1}\,K^{-1}$)
SL	laminar flame velocity (m/s)
T	temperature (°C)
U_f	fuel utilization
V	operation voltage (V)
Δh	enthalpy difference ($kJ\,mol^{-1}\,kg^{-1}$)
Δg	free energy difference ($kJ\,mol^{-1}\,kg^{-1}$)

Greek symbols

λ	excess air ratio (air/fuel ratio)
ρ	density ($kg\,m^{-3}$)
k	thermal conductivity of gas mixture ($W\,m^{-1}K^{-1}$)

Subscripts

a1	cathode off-gas temperature before pre-heater
a2	cathode off-gas temperature at inlet to after-burner
f1	anode off-gas temperature after pre-heater
f2	anode off-gas temperature at inlet to after-burner
g1	mixing chamber temperature
g2	flame barrier temperature
g3	flame barrier temperature
g4	combustion zone temperature

catalytic burner. Chachuat et al. [10] designed and optimized a man-portable SOFC-based power generation device consisting of a fuel processing reactor, a SOFC and two burners. In the proposed device, one burner was fed with the anode and cathode effluents for catalytic oxidation and the other burner is fed with a mixture of butane for catalytic oxidation to produce heat to maintain the stack at a sufficiently high temperature.

Porous media burners have emerged as a viable means of improving the system efficiency and eco-friendliness of a variety of heating systems. Compared to conventional combustion systems, porous media burners have a number of significant advantages, including lower emission, wide variable dynamic power range, high combustion stability, free choice of the geometry, and so forth. As a result, porous burner technology has been applied to a variety of applications in recent years, including household and air heating systems, gas turbine combustion chambers, independent vehicle heating systems, steam generators, and so forth [11].

Babkin et al. [12] established five steady-state combustion regimes in an inert porous medium and clarified the effects of flame quenching on the propagation velocity of the stable flame through the porous matrix. Defining the modified Péclet number as $Pe = \frac{S_L d_m c_p \rho}{k}$, where SL is the laminar flame velocity, d_m is the equivalent porous cavity diameter, c_p is the specific heat capacity, ρ is the density and k is the thermal conductivity of the gas mixture, the authors showed that the flame propagates if $Pe \geq 65$, but is quenched if $Pe < 65$. Based upon this finding, the authors suggested that the Péclet number provides a suitable index for predicting the flash-back phenomenon in porous medium combustion systems. Howell et al. [13] reviewed the processes associated with non-catalytic combustion within porous media and presented the exhaust emissions and radiant output characteristics of both single-stage and multi-stage porous media burners.

Trimis and Durst [14] conducted two-section porous media zone experiments in which the two sections contained materials with different properties and porosities. The results showed that flame stability and low pollutant emissions could be obtained over a wide range of equivalence ratios. Delalic et al. [15] developed a porous burner in which a built-in heat exchanger was used to enhance the thermal capacity and to improve the flame stability. Liu and Hsieh [16] showed that the use of liquefied petroleum gas as a fuel provided an effective and fuel-efficient means of achieving a stable combustion process within a porous heating burner under both transient and steady-state conditions.

The Institute of Nuclear Energy Research (INER), Taiwan, recently constructed a 1 kW SOFC system comprising a natural gas reformer, a SOFC stack, an after-burner, a fuel heat exchanger and an air heat exchanger (see Fig. 1). In this system, the hot cathode off-gas exiting the SOFC is passed through a heat exchanger, where it preheats the fuel prior to its ingress into the SOFC, and is then flowed to the after-burner. Meanwhile, the hot anode off-gas, containing a relatively high percentage of unburned fuel, is fed directly to the afterburner and is burned with the cathode off-gas. The hot flue gas exiting the after-burner is passed through a heat exchanger, where it preheats the air prior to entering the SOFC, and is then vented to the environment. In other words, the after-burner recovers the unspent energy from the fuel exiting the SOFC and uses this energy to minimize the load imposed on the anode- and cathode-side SOFC at the entrance side. Consequently, the after-burner not only limits the release of harmful emissions to the environment, but also yields an improvement in the overall efficiency of the SOFC system. Utilizing this system, Yen et al. [17] conducted a series of experiments to clarify the performance of the after-burner as a function of the fuel utilization (U_f,) when feeding the SOFC with hydrogen gas. The results showed that a continuous after-burner operation could be achieved by reducing the cathode off-gas temperature and maintaining a careful control of the flame barrier temperature within the burner.

The present study performs an experimental investigation into the optimal operating parameters of the after-burner within the 1 kW SOFC system shown in Fig. 1 for the case in which the SOFC is fed by a reformate gas rather than hydrogen. The remaining (unreacted) fuel relieved from anode exhaust of the SOFC is recuperated entirely and introduced itself. The summarized data of the SOFC stack are listed in Table 1. Twenty mbar of pressure drop caused by streams delivered through the SOFC unit is adopted. The detailed objectives of this study can be summarized as follows: (1) to evaluate the temperature distribution within the after-burner as a function of the SOFC fuel utilization, cathode off-gas temperature and excess air ratio, respectively; when feeding the SOFC with methane-based reformate gas; (2) to determine the cooling requirements for the after-burner; (3) to establish the optimal SOFC/after-burner operational settings, and (4) to clarify the respective effects of all the SOFC/after-burner system parameters on the burner operation so as to support the future development of an automatic burner control system.

The remainder of this paper is organized as follows. Section 2 describes the experimental apparatus and reviews the basic characteristics of the after-burner. Section 3 describes the use of the

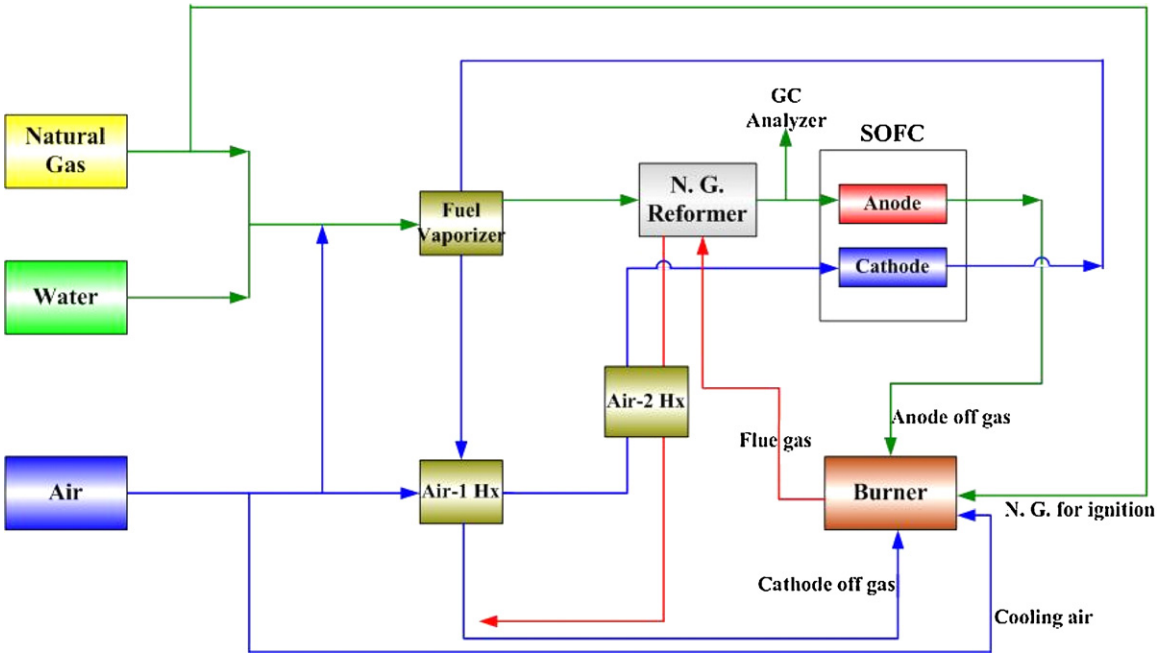

Fig. 1. Flow diagram of basic SOFC power system.

commercial GCTool software package [18] to simulate the compositions of the reformate gas, anode off-gas and cathode off-gas, respectively. Section 4 discusses the experimental conditions and procedures. Section 5 presents the experimental results and discussions. Finally, Section 6 provides some brief concluding remarks.

2. Experimental apparatus and after-burner characteristics

2.1. Experimental loop

Fig. 2 presents a schematic illustration of the experimental arrangement used to characterize the steady state and transient performance of the after-burner. As shown, the gas supply system comprised air, hydrogen, nitrogen, carbon monoxide, carbon dioxide, methane and liquid water, respectively. The cathode off-gas (air) was supplied by a compressor and was pre-heated to a specified temperature (T_{a2}) by pre-heater A (PH-A) before entering the burner. Meanwhile, the anode off-gas was produced by heating liquid water to the point of gasification in a pre-heater (PH-S) and then mixing the resulting steam with the hydrogen, nitrogen, carbon monoxide and carbon dioxide provided by the gas supply system. The anode off-gas was then heated by PH-A. The anode off-gas has a low volumetric heat capacity, and thus upon its release from PH-A, the fuel was flowed over electric heating tape (PH-F) to compensate for heat losses between the pipes. The desired temperature of the anode off-gas at the inlet to the after-burner, i.e. T_{f2}, was regulated using a Eurotherm PID controller. During the after-burner ignition and warm-up stage, the after-burner was supplied with methane via mass flow controller 7 (MFC-7). Finally, the after-burner was fed with additional air for cooling purposes via MFC-8.

During the experiments, the gas and liquid mass flow rates were controlled using a digital Alicat control unit. Meanwhile, the temperatures at various points in the experimental system were regulated by a Eurotherm PID controller. The temperature distribution within the after-burner was measured using four R-type thermocouples positioned in such a way as to record the temperatures in the mixing chamber (T_{g1}), the flame barrier zone (T_{g2} and T_{g3}), and the combustion zone (T_{g4}), respectively. A data acquisition system (DAS) was used to gather and record the system information in an automated fashion from the various measurement sources and to control the system operation using built-in software. Finally, the after-burner body and the adjacent piping system were insulated with a low thermal conductivity material in order to minimize heat losses.

Table 1
Summarized data of the basic type of SOFC stack.

Air temperature at stack inlet	700 °C
Fuel temperature at stack inlet	700 °C
Pressure drop in stack	20 mbar
Layers of stack	40
Electric work	1156 W
Cell voltage	0.7 V
Current density	400 mA cm^{-2}

2.2. Characteristics of after-burner

Fig. 3 presents a schematic diagram showing the heat transport within the after-burner used in the present experiments. As shown, the after-burner comprises a mixing chamber (Rg-1) and two porous-media sections, namely an upstream fine-pore section (Rg-2) and a downstream large-pore section (Rg-3). During operation, the flame stabilizes in the combustion zone (Rg-3) and a portion of the energy produced by the burned gases is transported back to the unburned mixture in the mixing chamber via the effects of thermal radiation and conduction. In practice, the occurrence of combustion within the after-burner depends on the pore size of the porous matrix structure in Rg-3. Specifically, the flame is quenched if the pore size is less than a certain critical dimension, but propagates within the porous matrix otherwise. From a physical perspective, the quenching phenomenon indicates that the heat generated by the combustion process is transferred to the porous matrix at a rate higher than it is produced, and thus the flame structure is extinguished.

To achieve a stable combustion process, the after-burner must be designed in such a way that the combustion process is confined to the large-pore section of the afterburner, i.e. Rg-3. Thus, unlike

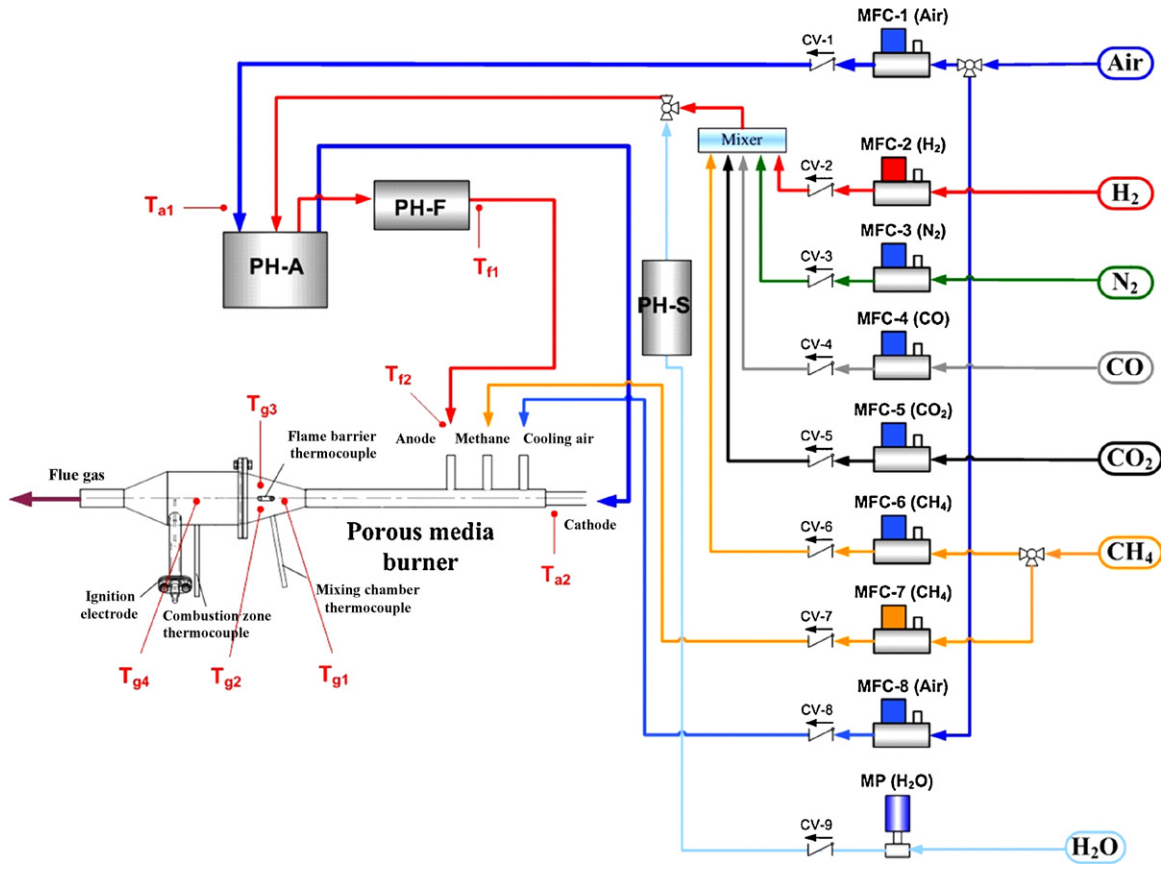

Fig. 2. Schematic of after-burner experimental apparatus.

traditional two-stage after-burners, in which the ignition electrodes are positioned between Rg-2 and Rg-3, in the after-burner used in the present experiments, the electrodes were installed toward the rear of the burner in order to reduce the risk of spark over. Furthermore, Rg-2 of the after-burner comprised a low porosity, low thermal conductivity material, while Rg-3 comprised a high porosity material with good thermal radiation and conducting properties. In designing the after-burner, the analyses considered the worst-case scenario in which the after-burner was fed with pure hydrogen, and specified the Péclet number as 30 in Rg-2 and 130 in Rg-3. In this way, the combustion process was confined within the pores of the porous structure in Rg-3, while Rg-2 served as a flame barrier zone to prevent the risk of flash back. Note that the flame barrier zone was also fed with cooling air as required in order to further minimize the risk of flame propagation toward the inlet region of the after-burner.

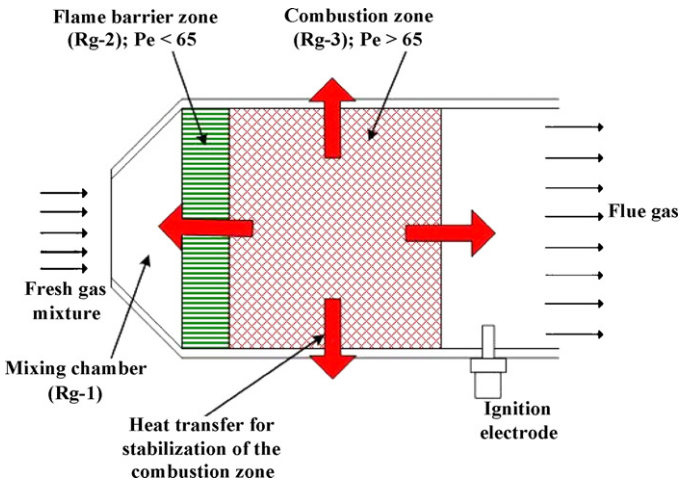

Fig. 3. Configuration of porous media after-burner.

In general, selecting an appropriate material for the porous matrices in a porous media afterburner is a crucial task. The materials should have the ability to withstand severe thermal and chemical stresses in order to prevent the possibility of cracking at elevated temperatures. Typical matrix materials include aluminum oxide (Al_2O_3), silicon carbide (SiC), zirconium dioxide (ZrO_2), and cordierite in the form of foam, lamellas or mixture structures. In the after-burner used in the present experimental trials, the flame barrier zone was constructed using a honeycomb cordierite structure with a porosity ratio of 33% and a pore diameter of 0.8 mm. Meanwhile, the combustion zone was fabricated using SiC in the form of metal foam with a pore density of approximately 10 pores per inch (ppi).

3. Simulation of reformate gas and SOFC exhaust gases using GCTool software

A general computational tool (GCTool) [18] developed by ANL is adopted to simulate the SOFC power-generation system in this paper. The primary models of the SOFC power-generation are SOFC stack, after-burner and reformer. The models provided in the GCTool used in this study are illustrated as follows [18].

3.1. SOFC stack

The enthalpy of the anode and cathode sides are evaluated by a given initial guess SOFC temperature and the required molar flow rate of oxygen to react in fuel cells are calculated by the spe-

cific fuel utility and fuel composition at the anode side entrance. Then, compositions, enthalpy, and entropy at outlets of the SOFC are obtainable at the particular operating pressure and temperature. The enthalpy difference, Δh, and free energy difference, Δg, between the inlet and outlet of the SOFC for the cell reaction can then be calculated as

$$\Delta h = h_{a,\text{out}} - h_{a,\text{in}} + h_{c,\text{out}} - h_{c,\text{in}} \quad (1)$$

$$\Delta g = \Delta h - T_{\text{cell}}(S_{a,\text{out}} - S_{a,\text{in}} + S_{c,\text{out}} - S_{c,\text{in}}) \quad (2)$$

where T_{cell} is the operating cell temperature and S represents for entropy. Then, the Nerst potential is calculated from

$$V_{\text{Nerst}} = e_0 + \left(\frac{RT_{\text{cell}}}{2F \ln (P_{a,\text{H}_2} \cdot P_{a,\text{CO}} \cdot P_{c,\text{O}_2} / P_{a,\text{H}_2\text{O}} \cdot P_{a,\text{CO}_2})} \right) \quad (3)$$

where F is Faraday's constant, P stands for the partial pressure for a specific species, R is the universal gas constant and e_o is the standard state potential for the cell. The actual cell voltage, V_{act}, is treated as input with the total overpotential and resistive losses, ΔV, determined from

$$\Delta V = V_{\text{Nerst}} - V_{\text{act}} \quad (4)$$

The cell current is calculated from

$$I = 4n_{\text{O}_2}F \quad (5)$$

The total electrical power is calculated from

$$P_{\text{elec}} = V_{\text{act}} I \quad (6)$$

An overall energy balance is made by iterating the exit temperature from the cell until the total enthalpy change of both flows across the cell are equal to the total electrical power. At each iteration over the cell temperature, all of the above calculations are redone. It is assumed that both flows leave the cell temperature. That is, $T_a = T_c = T_{\text{cell}}$ is varied until

$$h_{a,\text{in}} - h_{a,\text{out}} + h_{c,\text{in}} - h_{c,\text{out}} = P_{\text{elec}} \quad (7)$$

3.2. After-burner

Afterburner model is used to simulate the burner as oxygen and fuel or steam are mixed after exhausting from both sides of the SOFC to burn. Pressure drops in after-burner are neglected and the operation pressure of themselves is set to its own lower inlet pressure. Then, the heat of formation is estimated as follows when the needed oxygen flow rate depending on the composition of the fuel and a reference enthalpy with 298 K, 1 atm are determined.

$$\Delta h_{\text{form}} = \frac{(m_{\text{fuel}} + m_o)h + m_{\text{fuel}}\text{LHV}}{m_{\text{fuel}}} \quad (8)$$

where *LHV* is the lower heating value of the fuel, h is the reference enthalpy, m_{fuel} and m_o are fuel and oxygen mass flow rates, respectively. After burning, the enthalpy of the mixture can be determined from

$$h = \frac{m_{ox}h_{ox} + m_{\text{fuel}}\Delta h_{\text{form}}}{m_{ox} + m_{\text{fuel}}} \quad (9)$$

with the estimated values of enthalpy from Eq. (9) and pressure of the oxidizing flow, the flame temperature of the combustion products, as well as their equilibrium composition and other state variables can be determined.

3.3. Reformer

In general, natural gas can be reformed to a hydrogen-rich gas via steam reforming or a partial oxidation process. In the present experiments, the reforming process was performed using a combination of these two methods by feeding both steam and an oxidant (air) with the natural gas to a catalytic reactor. The composition of the resulting reformate gas was simulated using the GCTool tool box [18].

The catalytic reaction produced when steam reforming natural gas can be formulated as follows:

$$\text{CH}_4 + \text{H}_2\text{O} \rightarrow \text{CO} + 3\text{H}_2,\ \Delta H = 242\ \text{kJ mol}^{-1} \quad (10)$$

$$\text{CO} + \text{H}_2\text{O} \rightarrow \text{CO}_2 + \text{H}_2,\ \Delta H = -33\ \text{kJ mol}^{-1} \quad (11)$$

The reaction described in Eq. (10) is a slow and highly endothermic reaction, whereas that given in Eq. (11) is a rapid but weak exothermic water shift reaction in which the carbon monoxide is transformed to carbon dioxide and the hydrogen is transformed to water.

Meanwhile, the partial oxidation reforming of natural gas using oxygen as the oxidant can be formulated as follows:

$$\text{CH}_4 + 0.5\text{O}_2 \rightarrow \text{CO} + 2\text{H}_2,\ \Delta H = -247\ \text{kJ mol}^{-1} \quad (12)$$

In the INER 1 kW SOFC system (see Fig. 1), the combined steam reforming and partial oxidation process is performed at reformer temperature 760 °C. In addition, the flow rates of the water and oxidant are determined in accordance with a steam-to-carbon ratio (S/C) of 1.8 and an oxidant-to-carbon ratio (O/C) of 0.33. Utilizing a micro gas chromatography (GC) technique, the dry base composition of the reformate gas in the INER SOFC system was determined to be as follows: 65.2% hydrogen, 17.9% carbon monoxide, 12.6% nitrogen and 4.3% carbon dioxide. Table 2 compares the experimental measurements for the reformate gas composition with the simulation results obtained using GCTool. It is evident that a good agreement exists between the two sets of results, and thus the validity of the GCTool for prediction purposes is confirmed. As a result, GCTool was also used to predict the compositions of the anode off-gas and the cathode off-gas for various values of the SOFC fuel utilization (U_f).

In simulating the compositions of the anode off-gas and cathode off-gas, respectively, the enthalpies of the anode and cathode sides were evaluated for a given initial SOFC temperature. In addition, the molar flow rate of the air into the cathode side of the SOFC was calculated in accordance with the specified value of the fuel utilization (U_f) and the composition of the fuel at the anode side entrance. The composition, enthalpy, and entropy of the anode off-gases and cathode off-gases were then simulated at the corresponding pressure 1.2 atm and temperature 700 °C of the INER SOFC system. Table 3 summarizes the simulation results obtained for the compositions of the anode off-gas and cathode off-gas ($\lambda = 2$) for values of U_f in the range 0–0.6. The data presented in Table 3 were then used to set the compositions of the input gases to the experimental after-burner (see Fig. 2) in order to investigate the after-burner performance for various values of the SOFC fuel utilization.

4. Experimental procedures

4.1. Burner start-up

Before conducting the experiments, the after-burner was flushed with sufficient air and all connections were checked for leaks. Since anode off-gas compositions with a high fraction of hydrogen pose a significant explosion risk, the after-burner was ignited using methane gas. In the ignition process, mass flow controller 1, i.e. MFC-1 (see Fig. 2), was set such that air was supplied to the after-burner at a rate of 50 LPM and the ignition system was activated for 10 s, during which time the after-burner was also supplied with methane by MFC-7 at a rate of 4 LPM. By observing the temperature rise in the combustion zone (T_{g4}) and in the flame barrier region (T_{g2} or T_{g3}), the flame was moved downstream by carefully increasing the air supply. Having obtained suitable oper-

Table 2
Comparison of measured data and predicted data for composition of reformate gas.

	H_2 (Vol.%)	CO(Vol.%)	N_2(Vol.%)	CO_2(Vol.%)	Total
Micro GC measured	65.2% (16.6 LPM)	17.9% (4.6 LPM)	12.6% (3.2 LPM)	4.3% (1.1 LPM)	100% (25.5 LPM)
GCTool prediction	63.4% (16.1 LPM)	19.2% (4.9 LPM)	13.4% (3.4 LPM)	4.1% (1.0 LPM)	100% (25.4 LPM)

Table 3
Predicted compositions of anode off-gas and cathode off-gas ($\lambda = 2$) for fuel utilizations in the range $U_f = 0$–0.6.

	Anode off-gas (H_2, CO, CO_2, N_2: LPM, H_2O: cc min^{-1})					Cathode off-gas (N_2, Air: LPM)	
U_f	H_2	CO	H_2O	N_2	CO_2	Air	N_2
0	16.1	4.9	3.4	3.4	1.0	99.8	0.0
0.1	14.5	4.4	4.8	3.4	1.5	94.8	4.0
0.2	12.9	3.9	5.7	3.4	2.0	89.8	7.9
0.3	11.3	3.4	6.9	3.4	2.5	84.8	11.9
0.4	9.7	2.9	8.1	3.4	3.0	79.8	15.8
0.5	8.1	2.4	9.3	3.4	3.6	74.8	19.8
0.6	6.4	1.9	10.5	3.4	3.9	69.8	23.7

ating conditions (T_{g4} at 1000 °C), the methane gas was gradually replaced by a dilute gas comprising 20% H_2 and 80% N_2 flowed at a rate of 20 LPM.

4.2. Pre-heating of anode and cathode off-gases

As described in Section 2.1, the experimental system incorporates three pre-heaters, namely PH-A, PH-F and PH-S, to heat the anode and cathode off-gases such that temperatures T_{f2} (anode off-gas) and T_{a2} (cathode off-gas) reach their preset values, namely 650 °C and 390, 400, 450 or 500 °C, respectively.

4.3. Test conditions

Having heated the system, a series of experiments were performed in which the dilute gas was replaced by anode off-gas and cathode off-gas with the compositions shown in Table 2. Since the burner is designed to operate on an anode off-gas, it should not be operated long term using only natural gas. Furthermore, the flame barrier temperature should be carefully controlled within a certain range in order to minimize the risk of overheating, flash back or flame extinction. Finally, for mixing chamber temperatures greater than 500–575 °C, additional cooling air may be required to prevent flash back. The critical mixing chamber temperature depends mainly on the composition of the anode off-gas.

5. Experimental results and discussions

This section commences by reviewing the experimental findings presented by the current group in [17] for the case in which the SOFC system shown in Fig. 1 was fed using hydrogen. The section then presents and analyzes the results obtained in this study for the after-burner performance given the case where the SOFC system is fed with methane-based reformate gas.

5.1. Hydrogen anode off-gas

In [17], the present group conducted a series of after-burner experiments using hydrogen as the anode off-gas. In performing the experiments, an assumption was made that the SOFC exhaust gases entered the burner directly, and thus the anode off-gas and cathode off-gas temperatures were set initially as 650 °C and 700 °C, respectively. Meanwhile, the flame barrier temperature was maintained at 600 °C to prevent flash back. The experimental results showed that the burner required a significant cooling air flow to maintain a suitable operating temperature when the SOFC was operated with fuel utilizations in the range $U_f = 0$–0.6. However, the results also showed that the long-term economy of the after-burner operation could be improved by reducing the cathode off-gas temperature and increasing the flame barrier control temperature. Specifically, it was shown that by increasing the flame barrier temperature to 700 °C and reducing the cathode off-gas temperature to 330 °C, the burner could be operated without the need for additional cooling air when the SOFC fuel utilization was specified as $U_f = 0.6$ and the excess air ratio (i.e. the air/fuel ratio) was set to $\lambda = 2$. However, during the burner start-up stage, system heating up and the fuel transition period, additional natural gas and cooling air were required for the SOFC operation of the burner and the flame barrier temperature should be controlled in the range 600–650 °C. Fig. 4 illustrates the time-based variation of the temperature distribution within the after-burner for the optimal long-term anode and cathode off-gas temperature settings of 650 °C and 330 °C, respectively, and an excess air ratio of $\lambda = 2$. Note that in this figure, Phase I, Phase II and Phase III correspond to the warm-up period, the fuel transition period, and the long-term operation period, respectively. The figure also illustrates the corresponding flow rates of the cooling air, the methane ignition gas, and the hydrogen anode off-gas.

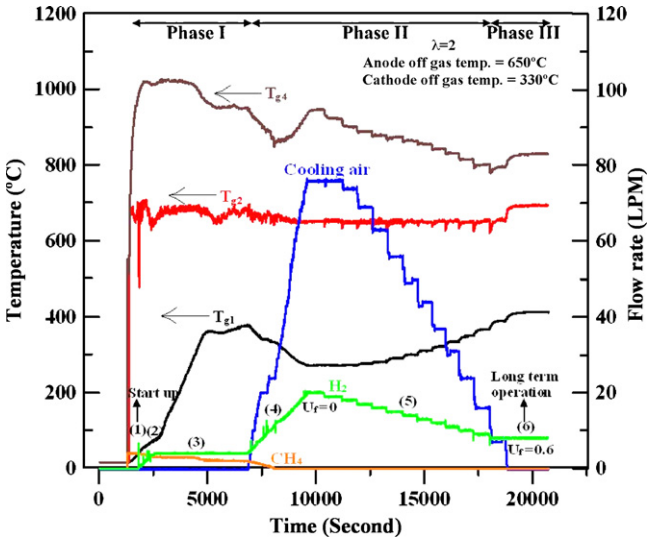

Fig. 4. After-burner temperature distribution and corresponding flow rates from system start-up to long-term operation. (Note that the SOFC is fed with hydrogen.)

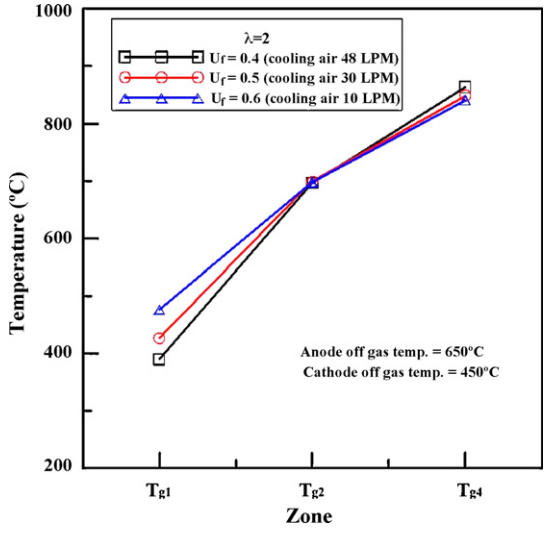

Fig. 5. After-burner temperature distribution for various values of U_f in range 0.4–0.6 and constant flame barrier temperature (T_{g2}) of 700 °C.

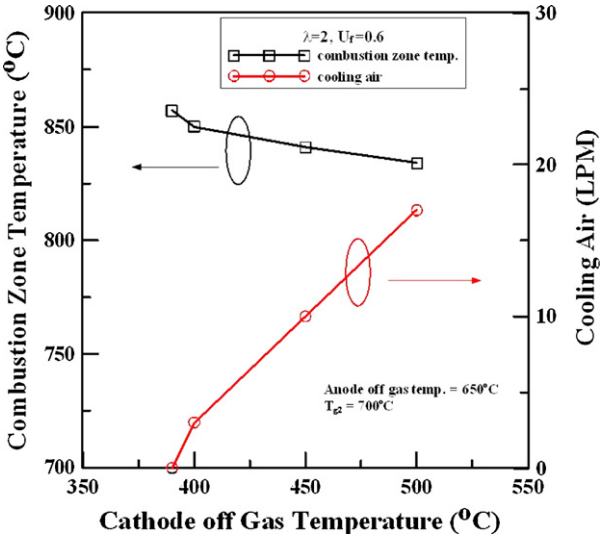

Fig. 6. Effect of cathode off-gas temperature on combustion zone temperature and cooling air flow rate required to maintain constant flame barrier temperature (T_{g2}) of 700 °C.

The results clearly show that following the completion of the fuel transition process, a long-tem operation can be obtained without the need for an additional cooling air flow.

5.2. Reformate gas anode off-gas

5.2.1. Effects of fuel utilization, cathode off-gas temperature and excess air ratio on long-term burner operation

In the present study, a series of experiments were performed using methane-based reformate gas as the SOFC fuel to investigate the effects of the fuel utilization (U_f), cathode off-gas temperature, and excess air ratio (λ) on the temperature distribution within the after-burner and the corresponding requirement for an additional cooling air flow. Fig. 5 illustrates the effect of the fuel utilization of the SOFC stack on the temperature distribution within the burner for a cathode off-gas temperature of 450 °C and an excess air ratio of $\lambda = 2$. Note that in performing the experiments, the anode off-gas temperature was set as 650 °C, cathode off-gas temperature 450 °C respectively and the flame barrier zone temperature was maintained at a constant $T_{g2} = 700$ °C. In general, a lower SOFC fuel utilization implies that a lower electric power is produced and a greater amount of unburned fuel enters the porous burner. As a result, the temperature within the burner increases, and thus additional cooling air is required to control the temperature of the flame barrier. In the present experiments, it was found that although the amount of additional air required for cooling purposes reduced with an increasing fuel utilization, additional air was required at all values of the fuel utilization in the considered range of $U_f = 0$–0.6.

Fig. 6 illustrates the effect of the cathode off-gas temperature on the combustion zone temperature and the flow rate of the cooling air required to maintain a constant flame barrier temperature of 700 °C. Note that the experiments were performed using an anode off-gas temperature of 650 °C, an excess air ratio of $\lambda = 2$, and a fuel utilization of $U_f = 0.6$. The results show that when the cathode off-gas temperature is reduced to 390 °C, the combustion zone temperature increases to 857 °C and the flame barrier temperature can be maintained at 700 °C without the need for additional cooling air. In other words, a cathode off-gas temperature of 390 °C not only increases the combustion zone temperature, and therefore maximizes the heat available to pre-heat the cathode gas (air) at the input to the SOFC, but also avoids the requirement for an additional cooling air supply, and therefore enhances the overall efficiency and economy of the SOFC/afterburner system. The lower value of the cathode off-gas temperature required to avoid the need for additional cooling air when running the SOFC on hydrogen (i.e. 330 °C, see Section 5.1) reflects the fact that the flame velocity of hydrogen is higher than that of CO.

Fig. 7 shows the effect of the excess air ratio on the combustion zone temperature and the cathode off-gas temperature required to avoid the need for cooling air. The results show that for excess air ratios of 1.5, 2.0 and 2.5, the requirement for additional cooling air can be avoided by setting the cathode off-gas temperature to 245 °C, 390 °C and 450 °C, respectively. In addition, it can be seen that the combustion zone temperature increases with a reducing value of the excess air ratio. At an excess air ratio of 1.5, the combustion zone has a temperature 875 °C. In general, a higher combustion zone temperature is desirable from a practical point of view since it increases the heat energy available to pre-heat the cathode gas prior to its ingress into the SOFC. However, the low value of the excess air ratio implies the presence of a high hydrogen concentration in the mixing region of the after-burner, and there-

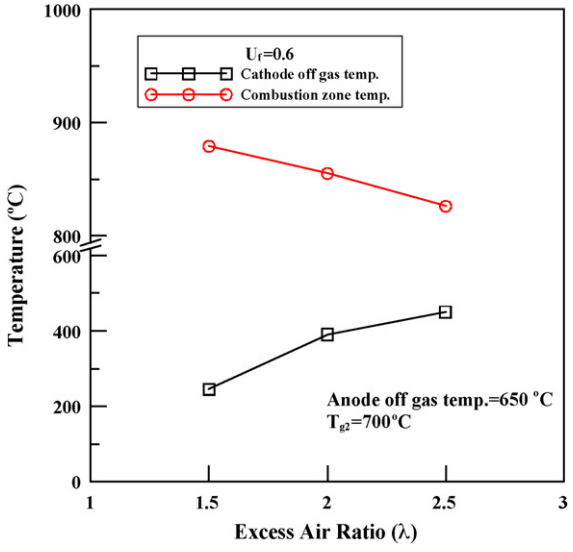

Fig. 7. Effect of excess air ratio (λ) on combustion zone and cathode off-gas temperature required to maintain constant flame barrier temperature (T_{g2}) of 700 °C without the need for a cooling air flow.

fore increases the risk of flash back. Furthermore, it was observed in the experiments that when the excess air ratio was specified as 1.5, the flame propagated in the upstream direction during the fuel transition stage, and prevented stable combustion from taking place within the porous matrix. As a result, an excess air ratio of 1.5 was deemed to be unsuitable from an operational point of view. Similarly, an air excess ratio of 2.5 was found to produce a relatively low combustion zone temperature 825 °C. Accordingly, the optimal value of the air excess ratio was determined to be $\lambda = 2$, giving rise to a combustion zone temperature 855 °C.

Overall, the results presented in Figs. 5–7 indicate that an optimal long-term operation of the INER SOFC/after-burner system can be obtained by specifying an anode off-gas temperature of 650 °C, a cathode off-gas temperature of 390 °C, a flame barrier temperature of 700 °C, an excess air ratio of 2 and a fuel utilization of $U_f = 0.6$.

5.2.2. *After-burner characteristics from start-up to long-term operation*

In general, the operating cycle of the after-burner integrated with the SOFC stack transits through three distinct phases, namely

(1) Phase I: Burner ignition to system heating up with dilute gas
(2) Phase II: Transition from dilute gas to anode off-gas and cathode off-gas with U_f increasing from 0–0.55.
(3) Phase III: Long-term operation with $U_f = 0.6$.

Fig. 8 illustrates the time-based variation of the temperature distribution within the after-burner when operated with the optimal settings given in Section 5.2.1. The corresponding variation in the flow rates of the cooling air and the anode off-gas, respectively, are also shown for reference purposes. During Phase I, i.e. the ignition and warm-up phase, the after-burner is supplied with methane gas and its temperature increases accordingly. During this phase the supply of methane is inevitable. However, once the combustion chamber temperature stabilizes, the methane gas is replaced by the anode off-gas and cathode off-gas with compositions regulated in accordance with Table 2 as the fuel utilization of the SOFC stack is progressively increased from $U_f = 0$ to $U_f = 0.6$. In this operational phase, i.e. Phase II, the supply of methane is not required. However, the after-burner must be supplied with cooling air to maintain the flame barrier temperature at around 650 °C. It can be seen that the flow rate of the cooling air reduces as the fuel utilization approaches the specified final value of $U_f = 0.6$. Finally, in Phase III, i.e. the long-term operational phase, the flame barrier temperature stabilizes at a value of 700 °C, and the after-burner operates without the requirement for cooling air or for any additional methane fuel.

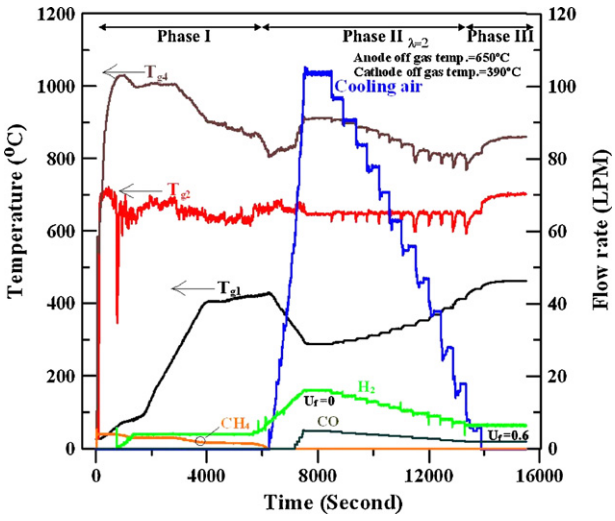

Fig. 8. After-burner temperature distribution and corresponding flow rates from system start-up to long-term operation. (Note that the SOFC is fed with reformate gas.)

6. Conclusions

This study has conducted an experimental investigation to establish the optimal operating parameters for an after-burner integrated with a 1 kW SOFC fed with reformate gas. The study commenced by using the commercial GCTool software package to predict the composition of the reformate gas given a knowledge of the reforming conditions. Having confirmed the validity of the simulation results via a comparison with the experimental measurements, GCTool was used to predict the compositions of the anode off-gas and cathode off-gas, respectively, for SOFC fuel utilizations in the range $U_f = 0$–0.6. The simulation data were then used to set the anode off-gas and cathode off-gas compositions in a series of experiments designed to establish the effects of the fuel utilization, cathode off-gas temperature and excess air ratio (λ) on the temperature distribution within the after-burner and the corresponding cooling air flow rate. The major conclusions of this study can be summarized as follows:

(1) The simulation results obtained for the composition of the reformate gas produced using a combined steam reforming/partial oxidation process are in good agreement with the experimental measurements. Hence, the feasibility of the GCTool package as a means of simulating the reforming reactions of natural gas is confirmed.
(2) Through an appropriate specification of the SOFC/after-burner operating conditions, a steady-state after-burner operation can be obtained without the requirement for additional cooling air or natural gas.
(3) During the ignition/warm-up phase, the after-burner must be supplied with natural gas rather than hydrogen-rich anode off-gas in order to prevent the risk of explosion. During this phase, the flame barrier temperature stabilizes at a value of around 600–650 °C without the need for cooling air. However, during the fuel transition stage, in which the methane gas is progressively replaced by the anode off-gas and cathode off-gas, cooling air is required to maintain the flame barrier temperature at around 600–650 °C. As the fuel utilization approaches a value of $U_f = 0.6$, and the compositions of the anode off-gas and cathode off-gas change accordingly, the requirement for a cooling air flow gradually reduces. In the steady-state operating phase, a stable flame barrier temperature of 700 °C is obtained, and the after-burner operates without the need for either cooling air or additional fuel.
(4) The experimental results obtained in this study give further insights into the combustion phenomenon within porous media after-burners and provide useful reference data against which to verify the results obtained using CFD (computational fluid dynamics) simulation packages for the temperature distribution within after-burners of a similar type.
(5) The test data presented in this study provide a useful starting point for the future development of an automated after-burner control system designed to optimize the performance of a SOFC system.

References

[1] A.J. Appleby, F.R. Foulker, Fuel Cell Handbook, Van Norstand Reinhold, New York, 1989.
[2] W.A. Stanley, Direct Energy Conversion, Allyn and Bacon, Inc, Boston, 1982.
[3] J. Larminie, A. Dicks, Fuel Cell Systems Explained, John Wiely & Sons, Ltd, England, 2000.

[4] P.E. Santangelo, P. Tartarini, Applied Thermal Engineering 27 (2007) 1278–1284.
[5] T.D. Chung, Y.P. Chyou, W.T. Hong, Y.N. Cheng, K.F. Lin, Energy & Fuels 21 (2007) 314–321.
[6] T.D. Chung, W.T. Hong, Y.P. Chyou, D.D. Tu, K.F. Lin, C.H. Lee, Applied Thermal Engineering 28 (2008) 933–941.
[7] C. Finnerty, G.A. Tompsett, K. Kendall, R.M. Ormerod, Journal of Power Sources 86 (2000) 459–463.
[8] S.H. Chan, C.F. Low, O.L. Ding, Journal of Power Sources 103 (2002) 188–200.
[9] E. Fontell, M. Jussila, J.B. Hansen, J. Palsson, T. Kivisaari, J.U. Nielsen, Wärtsilä–Haldor Topsøe SOFC Test System Extended abstract presented in SOFC-IX, Quebec Canada May 15–20, 2005.
[10] B. Chachuat, A. Mitsos, P.I. Barton, Chemical Engineering Science 60 (2005) 4535–4556.
[11] S. Moessbauer, O. Pickenaecker, K. Pickenaecker, D. Trimis, Fifth International Coference on Technologies and Combustion for a Clean Environment, Lisbon, Portugal, July 12–15, 1999.
[12] V.S. Babkin, A.A. Korzhavin, V.A. Bunev, Combustion and Flame 87 (1991) 182–190.
[13] J.R. Howell, M.J. Hall, J.L. Ellzey, Progress in Energy and Combustion Science 22 (1996) 121–145.
[14] D. Trimis, F. Durst, Combustion Science and Technology 121 (1996) 153–168.
[15] N. Delalic, Dz. Mulahasanovic, E.N. Ganic, Experimental Thermal and Fluid Science 28 (2004) 185–192.
[16] J.F. Liu, W.H. Hsieh, Combustion and Flame 138 (2004) 295–303.
[17] T.H. Yen, W.T. Hong, Y.C. Tsai, H.Y. Wang, W.P. Huang, C.H. Lee, The 3rd National Conference on Hydrogen Energy and Fuel Cell November 14–15, Tainan, Taiwan, 2008.
[18] GCTool, version 2.4, ANL Argonne IL (2001).